Circuit reorganization in the *Drosophila* mushroom body calyx accompanies memory consolidation

Lothar Baltruschat[1¶], Philipp Ranft[1¶], Luigi Prisco[1¶], J. Scott Lauritzen[2], André Fiala[3], Davi D. Bock[2,4] and Gaia Tavosanis[1,5*]

[1]Center for Neurodegenerative Diseases (DZNE), Bonn, Germany

[2]Janelia Research Campus, Howard Hughes Medical Institute, Ashburn, United States

[3]Molecular Neurobiology of Behaviour, University of Göttingen, Germany

[4] Department of Neurological Sciences, University of Vermont, Burlington, VT, USA

[5]LIMES Institute, University of Bonn, Germany

¶Equal contribution

**To whom correspondence should be addressed*

Short title: Structural and functional plasticity in the adult mushroom body

Keywords: Drosophila, structural plasticity, functional plasticity, memory consolidation, mushroom body, microglomerulus.

Summary

The capacity of utilizing past experience to guide future action is a fundamental and conserved function of the nervous system. Associative memory formation initiated by the coincident detection of a conditioned stimulus (CS, e.g. odour) and an unconditioned stimulus (US, e.g. sugar reward) can lead to a short-lived memory trace (STM) within distinct circuits [1-5]. Memories can be consolidated into long-term memories (LTM) through processes that are not fully understood, but depend on *de-novo* protein synthesis [6, 7], require structural modifications within the involved neuronal circuits and might lead to the recruitment of additional ones [8-17]. Compared to modulation of existing connections, the reorganization of circuits affords the unique possibility of sampling for potential new partners [18-20]. Nonetheless, only few examples of rewiring associated with learning have been established thus far [14, 21-24]. Here, we report that memory consolidation is associated with the structural and functional reorganization of an identified circuit in the adult fly brain. The formation and retrieval of olfactory associative memories in *Drosophila* requires the mushroom body (MB) [25]. We identified the individual synapses of olfactory projection neurons (PNs) that deliver a conditioned odour to the MB and reconstructed the complexity of the microcircuit they form. Combining behavioural experiments with high-resolution microscopy and functional imaging, we demonstrated that the consolidation of appetitive olfactory memories closely correlates with an increase in the number of synaptic complexes formed by the PNs that deliver the conditioned stimulus and their postsynaptic partners. These structural changes result in additional functional synaptic connections.

42 **Results**

43 To start addressing systematically the mechanisms that support memory
44 consolidation, we sought to investigate the properties of identifiable synapses in the
45 MB of the adult brain of *Drosophila* after the establishment of LTM. Within the main
46 MB input compartment, the calyx (MBC), PNs deliver olfactory information through
47 cholinergic synapses to the intrinsic MB neurons, the Kenyon cells (KCs) (Figure 1A).
48 In the MBC, large olfactory PN boutons are enwrapped by the claw-like dendrite
49 termini of ~11 KCs on average [26, 27], thereby forming characteristic synaptic
50 complexes, the microglomeruli (MGs) [28] (Figure 1A-E), which display functional and
51 structural plasticity in adaptation and upon silencing [29-31]. The pheromone and
52 odorant 11-cis-Vaccenylacetate (cVA) activates specifically those PNs that project
53 their dendrites to the DA1 glomerulus in the antennal lobe (AL) [32-34] (Figure 1A, B;
54 DA1-PNs). The DA1 glomerulus is mostly excluded from complex processing of
55 sensory information in the AL [35, 36], suggesting that by genetically marking the
56 DA1 PNs we could identify the individual boutons in the MBC that deliver the
57 olfactory response to cVA. We tested this by recording with volumetric calcium
58 imaging the response to odour stimulation in the MBC of animals expressing a
59 genetically encoded calcium indicator tethered at the KC postsynapses (*MB247-*
60 *homer::GCaMP3*) [30] in combination with a presynaptic fluorescent tag (*UAS-td-*
61 *Tomato*) expressed in DA1-PNs only (Figure 1C). Regions of interest (ROIs)
62 containing fluorescently labelled DA1-MGs showed a postsynaptic response
63 specifically tuned to cVA stimulation (84% of the fluorescently labelled MGs
64 responded to cVA only; n=7 animals, 72 boutons; Figure 1C).

65 Taken together, by selecting the combination of the cVA odorant and the DA1 subset
66 of PNs we established fly lines in which we can track a fly's neuronal response
67 towards a specific odour on the level of individual synaptic complexes in the MBC
68 (Figure 1A-C).

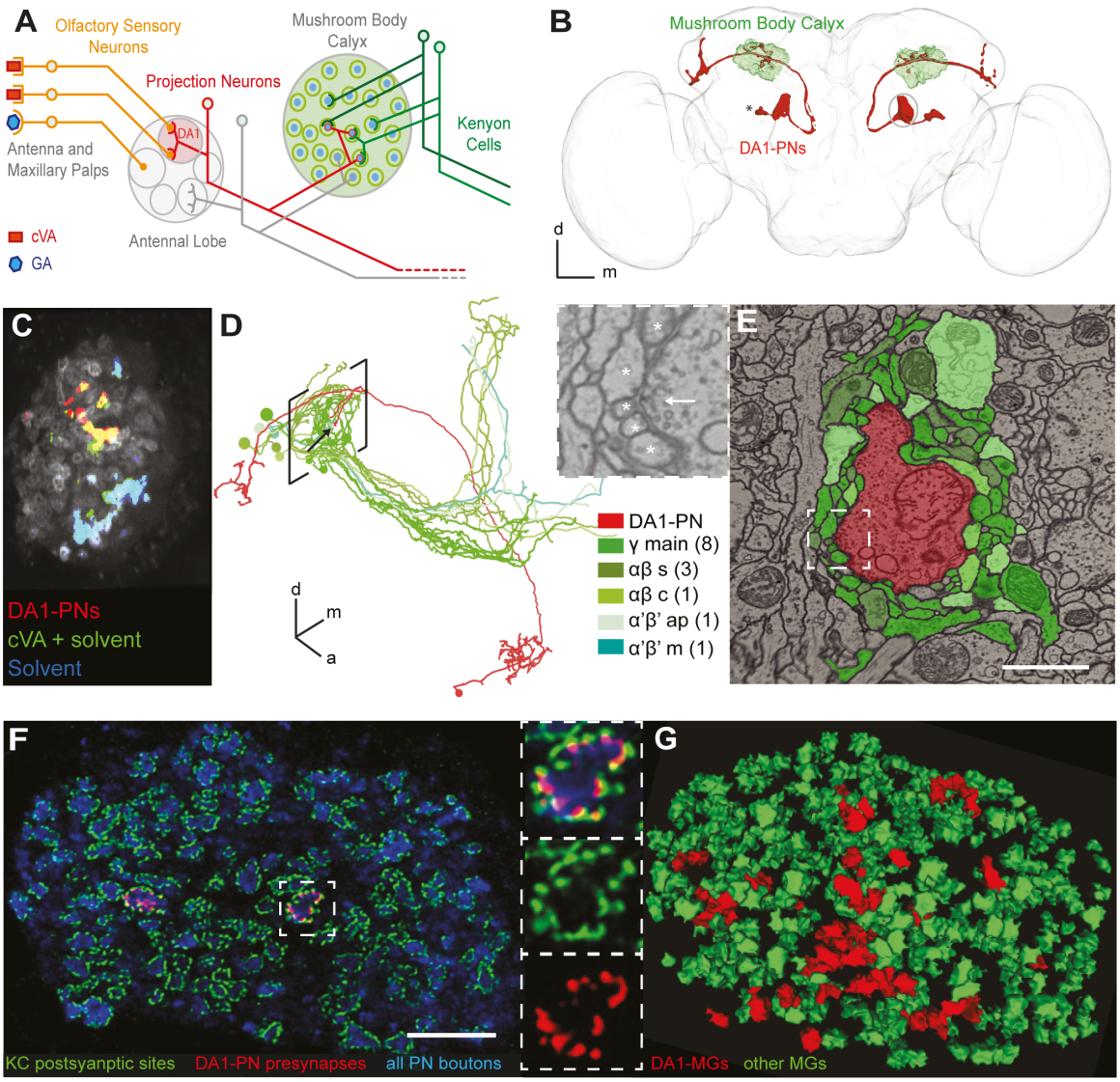

69

70 **Figure 1 | Identification of the synapses in the MBC responding to cVA odour**
71 **stimulation**

72 **(A)** Schematic representation of the olfactory circuit starting from the activation of specific
73 Olfactory Sensory Neurons (OSNs) by two exemplary odours cVA and GA. In the AL cVA-
74 responsive OSNs converge to the DA1 glomerulus (pale red), where they synapse onto DA1-
75 PNs (red). These deliver the cVA signal to the MBC via axon collaterals that terminate with
76 boutons forming large synaptic complexes, the MGs. Postsynaptic KCs are represented in
77 green. **(B)** Reconstruction from a full confocal serial section set of the DA1-PNs (red;

78 *R37H08-Gal4> UAS GAP43::Venus*); MBC (green; *MB247-Dα7::GFP*); DA1-PN cell bodies
79 (*); brain neuropil (light grey; α-synapsin antibody). **(C)** Volumetric calcium imaging of the
80 calyx of flies carrying *MB247-Homer::GCaMP3* (grey) and in which DA1-PNs are genetically
81 labelled (red; *R37H08-Gal4> UAS tdTomato*). cVA-elicited postsynaptic responses (green)
82 are specific to DA1-PNs, confirmed by the overlap between the two channels (yellow).
83 Generic response to the solvent (cyan= overlap of the responses to cVA+ EtOH, green, and
84 to EtOH only, blue). **(D)** Single DA1-PN (red) and the 14 KCs (green) postsynaptic to the
85 DA1-PN bouton indicated by the arrow. Tracings performed on the EM FAFB dataset [37].
86 Square brackets indicate location of MBC. Different green shades represent different KC
87 subtypes (as in E). Numbers in brackets in the legend represent the number of cells. **(E)**
88 Single EM section through the MG (arrow in D); scale bar = 1 µm. White square is magnified
89 in left top panel with arrow pointing to a T-bar of the AZ and * labelling fine dendritic
90 postsynaptic profiles of KCs. **(F)** Single plane confocal image of the MBC displaying PN
91 boutons (blue; α-synapsin antibodies); the PSDs of KCs (green; *MB247-Dα7::GFP*) and the
92 AZs of DA1-PN boutons only (red; *R37H08-Gal4 > UAS-brp-short*^{cherry}) identifying the cVA-
93 responsive MGs. Scale bar = 10 µm. The MG in the white square is magnified in the right
94 panels. **(G)** Automated 3D reconstruction of a confocal stack, including the image shown in
95 (F). The reconstruction of MGs is based on Dα7-GFP (green) (see also Figure S1) and MGs
96 receiving presynaptic input from DA1-PNs are marked by Brp–short^{cherry} (red). All other MGs
97 are in green. Full genotypes used and statistics for all Figures are included in the
98 Supplemental Genotypes and Statistics table.

99

100 To gain insight into the complexity of the MG microcircuit formed by a single DA1-PN
101 bouton we took advantage of the availability of a whole brain electron microscopy
102 (EM) volume of an adult female fly (FAFB) [37]. In this set of data we reconstructed a
103 complete MG connectome by tracing neurites from every pre- and postsynaptic
104 contact of a DA1-PN bouton until the corresponding neuron's identity was
105 anatomically determinable (Figure 1D, E; Supplementary Table 1). This particular
106 DA1-PN bouton made 33 excitatory, cholinergic contacts, all polyadic and identifiable
107 by the presence of a T-bar and of a synaptic cleft (Figure 1E, inset), apposed to 277
108 postsynaptic profiles. Most profiles (248) postsynaptic to the bouton originated from
109 14 KCs of 5 different subtypes: γmain (8), αβs (3), αβc (1), α'β'ap (1) and α'β'm (1)
110 [38](Figure 1D, E; Supplementary Table 1, Movie 1). γmain profiles were thus the
111 most abundant, although DA1-PN boutons are located within a region of the MBC
112 predominantly occupied by αβs KCs [39]. Each KC contacted the bouton with a
113 single claw receiving 8 to 25 presynaptic inputs from the PN bouton, in line with

114 previous estimates [26, 31]. Within the MG, the bouton received presynaptic input
115 from 4 cells: two additional γmain KCs forming divergent triads that included a KC,
116 the PN bouton and the anterior paired lateral neuron (APL) [40]; APL itself and one of
117 the two Mushroom Body Calyx 1 neurons (MB-C1) (Supplementary Table 1 and
118 described elsewhere). Taken together, a single MG represents a highly complex
119 microcircuit, involving many neurons (19 in this example) of different types (here 8).

120 To investigate whether such a complex structure could undergo plastic changes, we
121 designed a setup to reveal and measure the properties of identifiable MGs following
122 olfactory conditioning.

123 In confocal images, we highlighted cVA responsive MGs in the MBC by expressing
124 only in DA1-PNs the presynaptic active zone (AZ) marker Brp-short^{cherry} (Figure 1F)
125 [29, 41]. The postsynaptic densities (PSDs) of KC dendrites were decorated by cell-
126 type specific genetic expression of a GFP-tagged Dα7 subunit of the acetylcholine
127 receptor (Figure 1F) [29]. MGs could thus be identified with a software-based
128 automated 3D-reconstruction tool exploiting the *MB247-Dα7::GFP* signal and were
129 then classified as DA1-PN positive if they additionally displayed Brp-short^{cherry} co-
130 labelling (DA1-MG; Figure 1G; Figure S1). Further, we established an appetitive
131 associative conditioning paradigm using cVA or geranyl acetate (GA) as CS in STM
132 or LTM paradigms (Figure 2A; Figure S2A-C; see Methods) and applied it to flies
133 expressing the reporters mentioned above (Figure 2B, F, J). Alternatively, we mock-
134 trained the flies by presenting each odour or the sugar reward at 2 min intervals to
135 avoid the formation of appetitive association (Figure 2A, B, F, J) [42]. GA was chosen
136 as it activates a separate and non-overlapping set of PNs in comparison to cVA [43]
137 and 5% EtOH was added to provide a food-related context to the starved flies (Figure

138 S2B) [36, 44]. To assess if MGs formed by DA1-PN boutons (DA1-MGs) underwent
139 morphological modifications after learning, we prepared for confocal imaging female
140 fly brains dissected at 1 min (STM) or at 24 h (LTM) after training. After STM
141 establishment (Figure 2B) the total number, MG volume and lumen volume of DA1-
142 MGs was unchanged in cVA conditioned (cVA CS+) flies compared to the GA
143 conditioned (GA CS+) or mock control groups (average MG numbers: mock 28.91;
144 GA CS+ 30.40; cVA CS+ 28.76; n= 10-17; Figure 2C-E). However, in the LTM
145 paradigm (Figure 2F) the MG volume and the lumen volume of DA1-PN MGs were
146 decreased in cVA CS+ flies compared to GA CS+ or to mock-control flies (Figure 2G,
147 H). In addition, the total number of DA1-MGs was increased (average MG numbers:
148 mock 27.31; GA CS+ 27.47; cVA CS+ 32.06; n= 18-32; Figure 2I). Thus, LTM, but
149 not STM, was accompanied by an input-specific structural reorganization of the MBC
150 circuit, including an increase in MGs number. These changes were specific to the
151 conditioned odour, as they did not appear in the DA1-MGs when the conditioned
152 odour was GA. These data suggest that the neurons delivering the CS form new
153 boutons, which are of smaller size and enveloped by KC claws.

154 Olfactory associative learning relies on the function of the Ca^{2+}/CaM-dependent
155 adenylyl cyclase Rutabaga [42, 45, 46] and a defining trait of LTM is its dependence
156 on protein synthesis [6, 47, 48]. Indeed, a mutation in the *rutabaga* gene (*rut*^{2080}) [49]
157 or feeding flies with the protein synthesis inhibitor cycloheximide (CHX) immediately
158 after training abolished LTM (Figure 2J; Figure S2D). Importantly, loss of *rut* function
159 or CHX feeding also suppressed the structural changes in the DA1-MGs supporting
160 the correlation between LTM formation and structural changes in the circuit (Figure
161 2K-M; Figure S2E-G).

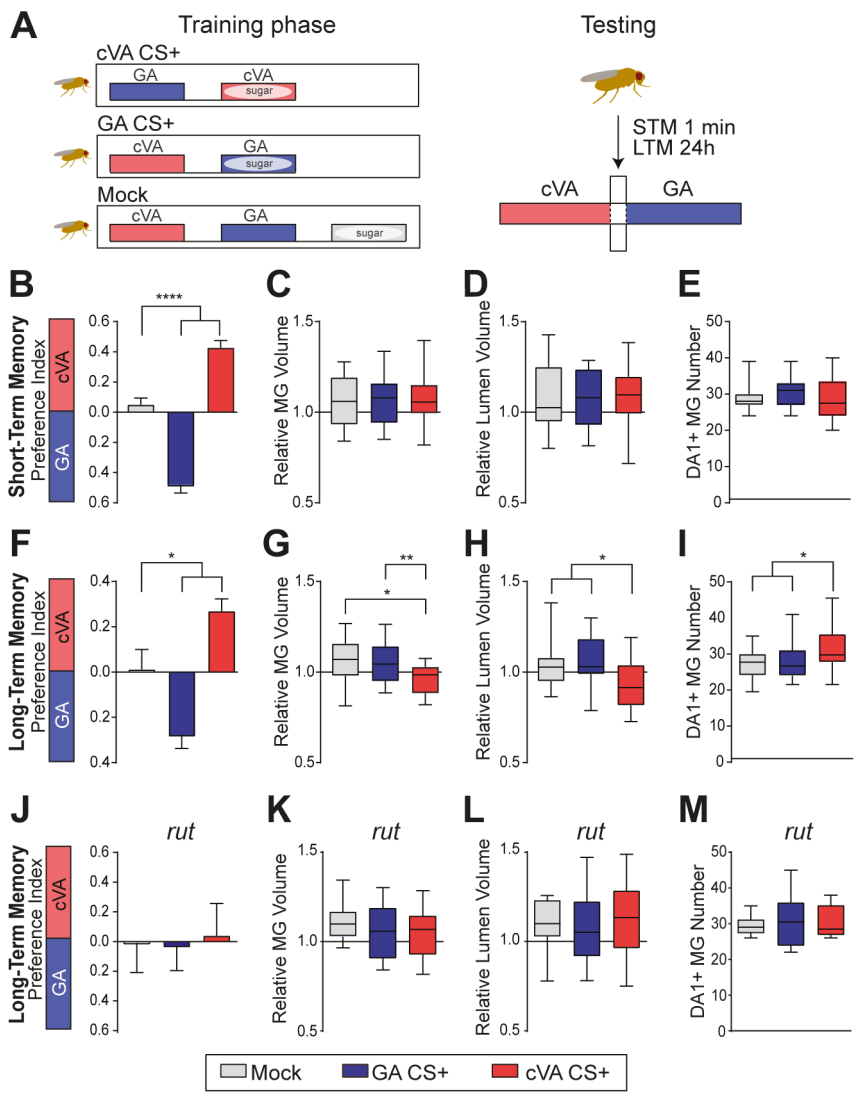

Figure 2 | Microglomeruli undergo structural changes upon appetitive long-term memory formation

(A) Schematic illustration of the appetitive conditioning paradigm. For training, the conditioned odour cVA (red box) or GA (blue box) is paired with sugar. In STM experiments flies are trained for 2 min with a 2 min interval between CS+ and CS- presentation and tested 1 min after training. In LTM experiments flies are trained for 5 min + 5 min with a 2 min stimulus interval and are tested 24 h after training. In the mock control the two odours and the sugar reward are presented in a temporally spaced sequence with a 2 min inter-stimulus pause. **(B, F, J)** Preference indices of flies *R37H08-Gal4/MB247-Dα7::GFP, UAS-brp-short*^{cherry} in the STM (n = 19 – 25) **(B)** or in the LTM (n = 14 - 19) paradigm **(F)** and preference index of *rut* mutant flies in LTM **(J)**, ($p > 0.05$, n = 17-18). Preference index values of the mock control group (grey bars) were compared to groups trained with GA CS+ (blue bar) or cVA CS+ (red bar). Multiple comparisons are tested throughout this study with one-way ANOVA with Bonferroni correction. Significance level is set at $p < 0.05$. *$p < 0.05$, ****$p < 0.0001$. In this and all other bar graphs, bars and error bars indicate mean and SEM, respectively. **(C, G, K)** MG volume is defined by the area enwrapped by the postsynaptic densities of KC dendrites. MG lumen volume **(D, H, L)** is the volume of the lumen as defined in Figure 1F. In STM the relative volume of DA1- MGs **(C)** and of their lumen **(D)** is not different between groups ($p > 0.05$; n = 15-20). In LTM the MG volume **(G)** and the lumen volume **(H)** of DA1- MGs in flies trained with cVA CS+ are smaller than in flies from the mock

183 control group or of flies trained with GA CS+ (* p < 0.05, **p < 0.01; *n* = 19–25). **(E, I, M)**
184 Number of DA1-PN positive MGs is unaffected in STM **(E)** (*p* > 0.05; n = 18 – 24). In LTM,
185 number of DA1-PN positive MGs in cVA CS+ trained flies is higher compared to flies of the
186 mock control or GA CS+ group **(I)** (*p < 0.05; n = 18-24)**. (K-L)** The structural modifications of
187 DA1- MGs in cVA CS+ trained flies after the appetitive LTM protocol were suppressed in *rut*
188 mutants (*p* > 0.05, n = 13–21). In all box plots in this and the following figures, the edges of
189 the boxes are the first and third quartiles, thick lines mark the medians, and whiskers
190 represent data range.

191

192 The increase in DA1-PN positive MG number after LTM formation with cVA CS+
193 suggests that new boutons might be formed during consolidation. To gain insight into
194 the cellular fundamentals of these modifications, we expressed in DA1-PN axons the
195 membrane-tagged fluorescent protein *UAS-GAP43::Venus* together with *UAS-brp-*
196 *short*^{cherry} and highlighted the postsynaptic densities on KC dendrites using *MB247-*
197 *Dα7::GFP* (Figure 3A-D). Serial optical sections of the MBCs of these flies trained
198 with cVA CS+, with GA CS+ or in the mock paradigm (Figure S2H) were used to
199 generate 3D reconstructions that were then aligned to a reference brain (JFRC2
200 [50]). The DA1-PN axons were then traced in the aligned high-resolution scans of the
201 MBC (Figure 3E). The DA1-PN boutons were highly clustered in the dorsal-posterior
202 part of the calyx [51], supporting the view that the localization within the MBC of DA1-
203 PN boutons is not entirely random (Figure 3F) [52]. The total length of DA1-PN
204 collaterals measured from the point where they leave the inner antennocerebral tract
205 (iACT) was increased in flies that had formed LTM after cVA CS+ training compared
206 to mock-control flies (Figure 3G). In addition, the total fraction of the MBC volume
207 containing DA1-PN positive boutons was increased in flies that had formed cVA CS+
208 LTM (Figure 3H). These observations suggest that during consolidation, additional
209 boutons are created by local growth at existing DA1-PN collaterals (Figure 3I).

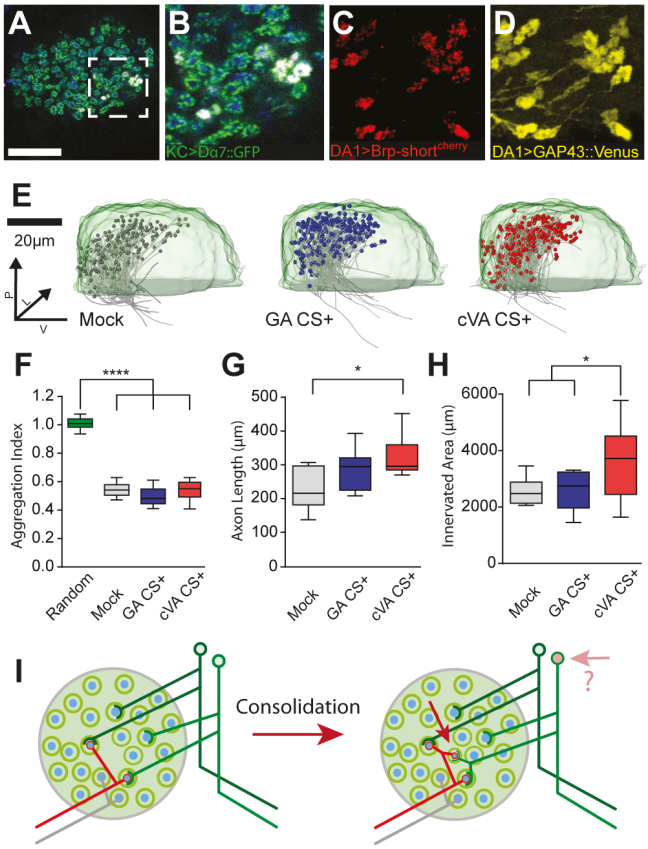

210

211 **Figure 3 | Modifications of axon collaterals and wiring properties of projection**
212 **neurons within the mushroom body calyx after long-term memory formation**

213 **(A)** Single optical section of the MBC of flies expressing Dα7GFP (green) in the KCs and
214 Brp-short^{cherry} (red) plus GAP43-Venus (yellow) in DA1-PNs (*R37H08-Gal4*); PN boutons
215 (blue; anti-Synapsin antibodies). **(B-D)** Magnification of the white square in (A) displaying the
216 merge as in A **(B)** or a maximum-intensity projection of Brp-short^{cherry} **(C)** or of GAP43-Venus
217 **(D)** signals. **(E)** Medial view of registered PN axons (grey) with traced boutons (grey, blue,
218 red spheres) within a standard calyx (light green). The registered PN traces are of mock
219 (grey), GA CS+ (blue) or cVA CS+ (red) trained groups. n = 10 for each group. **(F)** Boutons
220 are highly clustered independently of the treatment (Clark and Evans Aggregation index
221 compared to a hypothetical random distribution; ****$p < 0.0001$). **(G)** Total collateral axons
222 length of mock control, GA CS+ or cVA CS+ flies. (*$p < 0.05$; n = 10). **(H)** The convex hull
223 volume containing all DA1-boutons in the MBC per condition is increased in cVA CS+ flies
224 compared to mock control and GA CS+ group. **(I)** We suggest that the increased number of
225 MGs after consolidation is due to the formation of additional boutons responding to cVA. The
226 additional boutons form full MGs, as postsynaptic profiles of KCs surround them. It is unclear
227 whether this reorganization might lead to the recruitment of additional responding KCs (see
228 Discussion).

229

230 To address whether the observed structural changes within the MGs after LTM

231 impact on the functional representation of the CS in the MBC we analysed calcium

232 dynamics in KC dendrites. For this, we utilized flies carrying *MB247-homer::GCaMP3*

233 [30] in combination with volumetric calcium imaging (Figure 4A). We utilized this
234 simple genotype to guarantee that flies performed well in LTM experiments (Figure
235 S2I). We measured calcium response in the entire MBC volume during a single
236 odour application (5 s odour stimulation) of either cVA (1:400 in 5% EtOH) or EtOH
237 alone (5%). To identify areas with increased calcium dynamics during odour
238 stimulation we overlaid a grid consisting of 5x5 μm^2 ROIs over each optical section of
239 the volumetric time series. Based on the grid segmentation, we then calculated the
240 average $\Delta F/F\%$ for each ROI in the MBC. ROIs were classified as odour responsive
241 if the measured calcium response exceeded a set threshold ($\Delta F/F\% > 3x$ standard
242 deviation) during the first 2 s of stimulation (Figure 4B, C; Figure S3A, B). The
243 response pattern elicited specifically by cVA was defined after subtraction of the
244 EtOH response (Figure 4C; Figure S3C, D; see also Figure 1C). This approach
245 yielded a comprehensive picture of the functional odour response over time in the
246 MBC of trained or control flies (Figure S3D, E). After appetitive LTM formation, the
247 percentage of cVA-responsive ROIs was increased in cVA CS+ flies compared to the
248 mock control (Figure 4D) ($n = 7$, $p < 0.05$), suggesting that the additional DA1-PN
249 boutons are functionally connected to their postsynaptic KC counterparts and
250 capable of initiating a response in the postsynaptic KCs. We further analysed the
251 calcium dynamics over time of all animals of the mock or cVA CS+ group (Figure 4E,
252 F). Linear regression analysis of the fluorescence change during odour stimulation
253 showed a steeper drop of the linear fit in cVA CS+ flies ($R^2 = 0.6429$) towards
254 baseline compared to flies of the mock control group ($R^2 = 0.1124$). Besides, the
255 response towards the odour was more variable in mock-trained flies compared to the
256 cVA CS+ flies (Figure S3F). Initially (0-4s after start of stimulation), the total response
257 towards cVA stimulation was indistinguishable between mock control and cVA CS+

258 group. However, at subsequent time points (4-7s after start of stimulation) responses
259 were significantly lower in KC dendrites of the cVA CS+ group compared to the mock
260 control, showing a faster calcium decay towards the trained odour in CS+ flies (n = 7,
261 $p < 0.05$) (Figure S3G). Together, these data indicate a temporal sharpening of the
262 odour response.

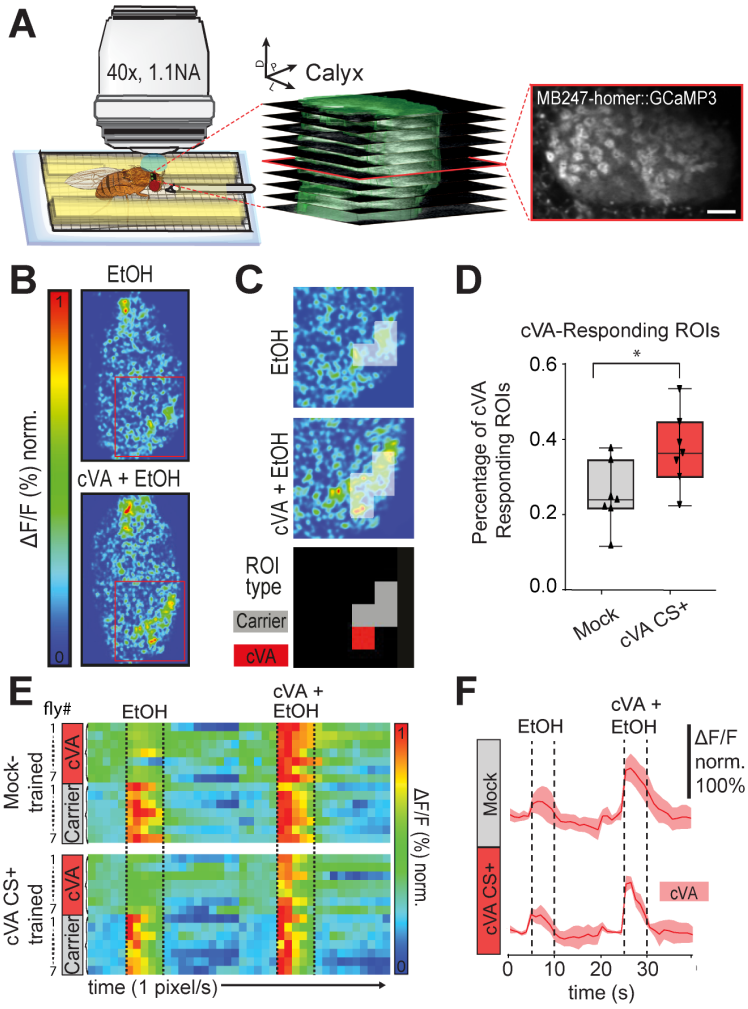

263

264 **Figure 4 | Long-term memory-induced functional plasticity in the mushroom**
265 **body calyx**

266 **(A)** Two-photon *in vivo* imaging setup. Schematic of a fly placed on a custom-made holder
267 under a two-photon microscope equipped with a 40x 1.1 NA water immersion objective. The
268 odour is delivered for 5s with a moisturized, constant air stream through a 1.2mm cannula.
269 (Central panel) Z series of the entire MBC volume of flies expressing post-synapse-tagged
270 Homer-GCaMP3 imaged during odour application at 1Hz (10 optical sections per volume,
271 4µm step size). (Right panel) A single slice of the image stack shown in the middle panel.

272 Scale bar = 10 µm. **(B)** Representative optical section from a volumetric time series showing
273 false-coloured response of KC dendrites to 5 s exposure to EtOH (top) or cVA + EtOH
274 (bottom). **(C)** Magnification of the red square area in (B). 5x5 μm^2 ROIs were classified as
275 cVA-responsive (red) if they were only active during cVA + EtOH application, but did not
276 respond to EtOH alone. **(D)** The percentage of cVA responsive ROIs increased after LTM
277 acquisition compared to the mock control (*$p < 0.05$; n = 7). **(E)** Dynamics of ΔF/F% changes
278 over time in KCs of *MB247-homer::GCaMP3* flies after mock training (top) or LTM acquisition
279 (bottom). Each row of the heat map represents average responses per animal of all cVA
280 responsive ROIs (pink) or of all carrier EtOH responsive ROIs (grey) within one MBC over
281 time. Each column represents one 1s. Flies are first exposed to the EtOH (5s) and then to
282 cVA + EtOH (5s) as indicated by the dashed lines. **(F)** Plot of average calcium dynamics over
283 time of cVA responsive ROIs during 5 s stimulation with EtOH or with cVA in EtOH (dashed
284 lines) in mock-trained (top) or cVA CS+ (bottom) flies (n = 7 per condition).

285 **Discussion**

286 We report input-specific reorganization of the adult MBC circuit associated with the
287 formation of long-term appetitive memory. By visualizing presynaptic markers in PNs
288 and the KC postsynaptic densities, we uncover an increase in the number of PN
289 boutons and at the same time reveal that these boutons are enveloped by KC
290 postsynaptic profiles, suggesting that new MGs are formed during memory
291 consolidation. These findings are particularly remarkable, given the high degree of
292 complexity of the MG microcircuits revealed by our EM reconstruction and including
293 the dendrite claws of multiple KCs of distinct subtypes. The cellular mechanisms
294 leading to the increased number of odour-specific complex MGs remain to be
295 clarified, but they will require a tight coordination between pre- and postsynaptic
296 partners. We suggest that they could be driven by intrinsic reactivation of KCs during
297 the consolidation phase [53, 54] or by modulatory inputs into the calyx [38, 55-58]. In
298 either case, we expect a complex pattern of activation that might be difficult to
299 reproduce in artificial settings [29, 59]. In agreement with our present report, the
300 density of PN boutons in the MBC increases after appetitive long-term conditioning in
301 honeybees and transiently also after avoidance learning in leaf-cutting ants [60, 61].
302 In comparison to those data, using genetic and functional identification of PN subsets

303 we reveal here that the structural modifications are specific and limited to the PNs
304 conveying the conditioned odour. Importantly, our *in vivo* functional imaging data
305 support the view that the circuit reorganization that we describe leads to additional
306 functional MGs responding to the conditioned odour. Additionally, they demonstrate a
307 specific change in functional response in the KC dendrites towards the trained odour
308 as the calcium levels drop faster towards baseline after appetitive associative
309 conditioning. The faster decay kinetics could contribute to a more efficient temporal
310 summation of responses or refine the KC response [62]. They are in line with recent
311 data from appetitive conditioning experiments from the honeybee possibly rooted in
312 inhibitory modifications [63]. An important open question is the effect of the increased
313 number of responding MGs on the pattern of KC activation. KCs respond sparsely to
314 odour input and require the coincident activation of multiple of their claws to produce
315 an action potential [64]. Our data might underlie the addition of connections between
316 the active PNs and, preferentially, a set of already responding KCs, leading to
317 facilitated response to the conditioned odour, but without changing the set of
318 responding KCs. A recent publication suggests an exciting alternative view. After
319 aversive LTM establishment, the number of KCs responding to the conditioned odour
320 is increased [65]. If we hypothesize that appetitive conditioning could lead to a similar
321 outcome, our data could provide anatomical and functional support to these findings.
322 The combination of these data suggests that the pattern of KC response is
323 modulated by experience during the adult life of the animal and might represent a
324 rich signifier of sensory stimulus and context.

325 **Acknowledgements**

We thank K. Keppler, M. Schoelling, A. Mueller and J. C. Vijayakumar for technical assistance. We are grateful to C.B. Fisher, S.A. Calle-Schuler, N. Sharifi, B. Gorko, L. Kmecova, I.J. Ali, N. Masoodpanah, J. Hsu and F. Li in D. D. Bock's lab for their support in tracing evaluation. We thank Y. Aso, HHMI Janelia, the Kyoto Drosophila Genetic Resource Center and the Bloomington Stock Center for fly lines and FlyBase. We are grateful for their assistance to C. Moehl in the establishment of the cluster analysis, S. Dipt with initial calcium imaging experiments and R. Court for providing the brain aligner and support. We thank S. Sachse, D. Isbrandt, T. Hige, S. Remy, M. Nawrot, O. Barnstedt, the members of the Tavosanis lab for discussion and/or critical reading of the manuscript and B. Schaffran for help with video editing. L.B. acknowledges support by the Bonn International Graduate School of Neuroscience. This work was supported by the DFG FOR 2705 to G.T.

Author Contributions

L.B. and G.T. conceived the project and designed the experiments. L.B., P.R. and L.P. constructed fly strains, performed behavioural experiments, produced and analysed the anatomical data. J.S.L. and D.D.B. established the set of EM data and P.R. performed the tracings presented here. Scripts and routines for the analysis were established by L.B. and L.P. Functional imaging experiments were designed and performed by L.B and L.P. with support by A.F. The manuscript was written by G.T, L.B., P.R and L.P.

Competing Financial Interests statement

The authors declare no competing interests.

348 **Methods**

349 **EM reconstruction and identification**

350 Neuron skeletons were reconstructed in a serial section transmission electron
351 microscope (ssTEM) volume of a complete female adult *Drosophila melanogaster*
352 brain [37] and manually traced using CATMAID [66]. Thus, traced neuron skeletons
353 represent the branching of neurons and the location of their cell bodies and
354 synapses. Chemical synapses were manually annotated and identified consistently
355 with the criteria of other CATMAID-based *Drosophila* connectomic studies [37]: 1) an
356 active zone (AZ) surrounded by vesicles, 2) a presynaptic specialization (*e.g.* T-bar),
357 3) synaptic cleft and 4) a post synaptic density zone (PSD), which however can be
358 absent. If the PSD is absent, we annotated all cells along the synaptic cleft as
359 postsynaptic [37, 67]. Neuron identity is based on previously described morphologies
360 in light microscopy (KC subtypes, APL, MB-C1, PN), such as dendritic branching,
361 axonal projection and location in the neuropil [38, 40, 52, 68, 69]. Additionally, we
362 performed a neuron search against a light microscopy dataset in NBLAST [70], as
363 described in [37] for PN subtype identification. 3D reconstructions of the PN bouton
364 and KC claws from ssTEM sections were created manually with the ImageJ plugin
365 TrakEM2 [71].

366 **Fly strains**

367 Flies were raised at 25°C, 60% relative humidity in a 12h/12h light-dark cycle on a
368 standard cornmeal-based diet. Individual insertions are listed below. Detailed
369 information on genotypes used in this study is listed in the Supplemental Genotypes
370 and Statistics table.

371

Insertion	Source	Reference
R37H08-Gal4	Kind gift of Y. Aso, HHMI, Janelia	FlyBase: FBti0191253
P{UASp-Venus.GAP43}10	Bloomington Drosophila Stock center	FlyBase: FBti0129930

P{UAS-tdTom.S}2	Bloomington Drosophila Stock center	FlyBase: FBti0145103
P{ry[+t7.2]=IArB}rut[2080]	Kind gift of A. Fiala, Uni Goettingen	[49] FlyBase: FBti0003267
P{UAS-GCaMP3.homer}	Kind gift of A. Fiala, Uni Goettingen	[30]
MB247-Dα7::GFP	Lab stock collection	[29]
UAS-brp-short^{cherry}	Lab stock collection	[29]

372

373 **Behaviour**

374 All experimental steps were performed at 23°C, 60% relative humidity using mixed
375 populations of *Drosophila* males and females maintained in a 12h/12h light/dark
376 cycle. Flies were collected 0-4d after eclosion, starved for 24 hours on wet paper
377 tissue (Kimberly-Clark Worldwide Inc.) allowing for water uptake and then trained. In
378 appetitive memory experiments ~80 flies were first exposed to an odour (CS-) alone
379 (2min in short- and 5 minutes in long-term memory experiments). After a 2min inter-
380 stimulus pause flies were trained by receiving dry sucrose on filter paper (3M Chr,
381 Whatman) paired with a second odour (CS+) (2min in short- and 5 minutes in long-
382 term memory experiments). 5 minutes of sugar availability improved the survival of
383 flies undergoing the LTM paradigm. In mock controls, all stimuli used in the
384 associative conditioning experiment were presented separately. Flies were tested
385 after 1min retention time for short- or after 24h retention time for long-term memory.
386 During the 24h retention flies were deprived of food and maintained in tubes
387 containing moist paper tissue. During the test flies were allowed to choose between
388 CS+ and CS- odours in a T-maze for 2min. A preference index (PI) was then
389 calculated as the ratio of the difference between the number of flies that chose the
390 CS+ and those that chose the CS- odour and the total number of flies: $PI =$
391 $\frac{(CS+)-(CS-)}{(CS+)+(CS-)}$. Odours used for conditioning were 11-cis vaccenyl acetate (Cayman

392 Chemicals) 1:400 in 5% EtOH in PBS, geranyl acetate (Sigma Aldrich) 1:100 in 5%
393 EtOH in PBS or 5% EtOH in PBS. EtOH was necessary to provide a food-related
394 context to the starved flies (Figure S2B).

395 **De-novo protein synthesis inhibition**

396 Immediately after training, flies were fed 35 mM cycloheximide (Sigma-Aldrich) [6]
397 dissolved in 125mM sucrose and 0.01% carmine solution for 30min. The red dye
398 carmine allowed confirming rapid drug uptake. A control group fed with 125mM
399 sucrose and 0.01% carmine (Sigma-Aldrich) solution showed no learning defects.

400 **Immunohistochemistry**

401 2-5 flies were randomly picked from conditioning experiments right before testing.
402 Brains of females were dissected in cold phosphate-buffered saline (PBS) with 0.05%
403 Triton and subsequently fixed in PBS containing 4% formaldehyde at RT for 50 min.
404 After fixation brains were washed in PBS with 0.3% Triton before incubation
405 overnight at 4°C with the following primary antibodies all diluted in PBS with 0.3%
406 Triton: rabbit anti-RFP (1:2000; Rockland), rabbit anti-GFP (1:200; Life
407 Technologies), mouse monoclonal anti-synapsin (3C11, 1:100; DSHB), mouse
408 monoclonal anti-β-Galactosidase (1:200 Abcam). After washing, the brains were
409 incubated with secondary antibodies in PBS containing 0.3% Triton for 4h at RT.

410 The secondary antibodies were Alexa Fluor568-conjugated goat anti-rabbit, Alexa
411 Fluor488-conjugated goat anti-rabbit, Alexa Fluor568-conjugated goat anti-mouse,
412 Alexa Fluor633-conjugated goat anti-mouse (all used 1:200 and from Life
413 Technologies). Brains were mounted in Vectashield (Vector) and imaged with a laser
414 scanning confocal microscope (LSM 780, Zeiss). For high resolution scans we used
415 a C Plan-Apochromat 63x/1,4 Oil objective (Zeiss) with a voxel size of
416 0.09x0.09x0.25μm^3 for quantitative analysis. Overviews of entire brains were taken
417 with an LCI Plan-Apochromat 25x/0.8 objective (Zeiss) at a voxel size of
418 0.55x0.55x1μm^3.

419 **Axon reconstruction**

420 To analyse axon and bouton distribution in the calyx, membrane-tagged Venus was
421 expressed in addition to the previously used markers under the control of a DA1-PN
422 Gal4-driver line (*R37H08-GAL4, UAS-Gap43::Venus / MB247-Dα7::GFP, UAS-brp-*
423 *short*^{cherry}). Brains of 10 female flies per condition were immunolabelled with anti-
424 synapsin antibodies (as above) and imaged. For PN axon reconstruction a high-
425 resolution scan (0.09x0.09x0.25µm^3, 63x NA1.4 oil immersion) of the right brain
426 hemisphere of female flies was acquired with a confocal microscope. In addition, an
427 overview scan used for registration was taken with a low magnification objective (25x;
428 NA 0.8 multi-immersion). PN axon reconstruction was performed on the high-
429 resolution scan of Venus signal in the trees toolbox available for Matlab [72]. In a
430 second step tracings and high-resolution images were aligned to the registered calyx.
431 For generation of a standard calyx with a volume of 37583 µm^3 (Figure 3E, light
432 green) the Dα7 signal of three registered calyces was averaged and reconstructed in
433 Amira using the segmentation editor. Next, tracings were aligned to the registered
434 overview scan in two steps. First, the iACT of the high-resolution image and of the
435 registered brain in the Venus channel were aligned. Next, the calyx volume of the
436 high-resolution calyx and the standard calyx went through a rigid registration
437 performed in Amira. The alignment parameters were then applied to the axon
438 reconstructions. Boutons were traced on the now registered high-resolution images
439 with the landmark function in Amira. Bouton distribution inside the MBC was
440 evaluated within a 3D grid of 10µm^3 cubes.

441 **Two-photon *in vivo* calcium imaging**

442 A mixed population of up to 4 d old *MB247-homer::GCaMP3* flies were starved for
443 18h at 22°C before appetitive conditioning with cVA (1:400, 5% EtOH in PBS), GA
444 (1:100, 5% EtOH in PBS) was used as CS-. Starved untrained flies displayed no bias
445 towards either of these odours at 24 hours. Flies used for imaging were randomly
446 picked from the trained group right before testing. They were used for imaging only if
447 the remaining flies from the same group had learned. For imaging, flies were briefly
448 anesthetized on a peltier element at 4°C, placed into a custom-built imaging chamber
449 (Figure 4A) and fixed using adhesive tape. The head capsule was opened under
450 Ringer´s solution (5 mM HEPES, pH 7.4, 130 mM NaCl, 5 mM KCl, 2 mM $CaCl_2$, 2
451 mM $MgCl_2$). To minimize movement brains were stabilized with 1,5% low melting

452 agarose (Thermo Scientific) in Ringer´s solution. Flies were imaged with a two-
453 photon laser-scanning microscope (LaVision BioTec, TriM Scope II) equipped with an
454 ultra-fast z-motor (PIFOC® Objective Scanner Systems 100µm range) and a Zeiss
455 C-Apochromat 40x, 1.1 NA water –immersion objective. Two-photon images were
456 analysed using Fiji/ImageJ [73]. GCaMP fluorescence was excited at 920 nm using a
457 Ti:sapphire laser (Coherent Chameleon). A stack consisting of ~ 10 optical sections
458 was taken at 1Hz in approximately 0,26x0,26µm xy- and at 4µm z- resolution. Odours
459 were applied with a constant humidified air stream (10ml/s) using a commercial
460 device (Stimulus Controller CS 55, Ockenfels SYNTECH GbmH) triggered 5s after
461 acquisition of the 1st frame by a multifunction I/O module (NI USB-6008), which was
462 controlled by Matlab (Data Acquisition Toolbox). To record DA1 neurons specific
463 responses, *UAS-tdTomato; R37H08-GAL4, MB247-Homer::GCaMP3* flies were
464 anesthetized on ice, positioned in a polycarbonate imaging chamber ([74]; gift from S.
465 Tomchik), and immobilized using Myristic Acid (Sigma-Aldrich). To allow optical
466 access to the Calyx, a small window was opened through the head capsule under
467 Ringer´s solution. Two-photon microscopy was conducted as described above.

468 **Two-photon image data processing**

469 The time series was processed with a custom Fiji/ ImageJ macro and corrected for
470 small x/y shifts with the StackReg plug-in [75]. A grid (ROIs, side length 5 µm) was
471 assigned for each optical slide of a stack covering the entire calyx. Intensity tables of
472 each square of the grid were exported to Microsoft Excel and the ΔF/F was
473 calculated. The baseline (F_0) was set by averaging the intensities within each ROI of
474 the 5 frames prior to odour stimulation. ROIs were regarded as responsive, if their
475 normalized ΔF/F% throughout the first 2s of odour application exceeded 3x the
476 standard deviation of the F_0 of the same ROI in the 5s (=5 images) before odour
477 stimulation. ROIs below that threshold were assigned into the category
478 “unresponsive”. ROIs calcium responses higher than the threshold were further
479 subdivided into three categories. The first category was “Carrier” (responsive to both,
480 5% EtOH and 1:400 cVA, 5% EtOH). The second category was “cVA” (responsive
481 only to 1:400 cVA, 5% EtOH and not to 5% EtOH) or “EtOH” (response only to 5%
482 EtOH application and not to 1:400 cVA, 5% EtOH). To analyse DA1 boutons
483 responses to 5% EtOH and 1:400 cVA+ 5% EtOH were recorded from naïve *UAS-*

484 *tdTomato; R37H08-GAL4, MB247-Homer::GCaMP3* flies, exported to Fiji/ ImageJ
485 and ROIs were manually drawn around DA1 boutons based on the tdTomato
486 fluorescence. Intensity values of each ROI were transferred to Microsoft Excel and
487 ΔF/F values were calculated using the average of the first 5 frames prior to odour
488 stimulation as baseline (F_0). Responsive ROIs were defined as above. These results
489 were age, gender and sequence independent as presenting the odours in a different
490 order did not change the results of the analysis. Calcium traces were generated in
491 Prism 7 (GraphPad Software).

492 **Statistics**

493 Statistical analyses were performed with Prism7.01 software (GraphPad). All data
494 were tested for normality (D'Agostino & Pearson omnibus normality test) and
495 homogeneity of variances (F-test). Comparisons of normally distributed data were
496 tested by a one-sample t test, a two-sample t test or one-way analysis of variance
497 (ANOVA) followed by planned, pairwise multiple-comparison tests with adjusted p-
498 values (Bonferroni), as shown in the Genotypes and Statistics table. Definition of
499 statistical significance was set to <0.05. Asterisks denote * $p<0.05$; ** $p<0.01$;
500 ***$p<0.001$; **** $p<0.0001$; n.s. not significant.

501 **References**

502 1. Josselyn, S.A., and Tonegawa, S. (2020). Memory engrams: Recalling the past and
503 imagining the future. Science *367*.

504 2. Boto, T., Stahl, A., and Tomchik, S.M. (2020). Cellular and circuit mechanisms of
505 olfactory associative learning in Drosophila. Journal of neurogenetics *34*, 36-46.

506 3. Wang, Y., Mamiya, A., Chiang, A.-s., and Zhong, Y. (2008). Imaging of an early
507 memory trace in the Drosophila mushroom body. The Journal of neuroscience : the
508 official journal of the Society for Neuroscience *28*, 4368-4376.

509 4. Liu, C., Placais, P.Y., Yamagata, N., Pfeiffer, B.D., Aso, Y., Friedrich, A.B., Siwanowicz,
510 I., Rubin, G.M., Preat, T., and Tanimoto, H. (2012). A subset of dopamine neurons
511 signals reward for odour memory in Drosophila. Nature *488*, 512-516.

512 5. Burke, C.J., Huetteroth, W., Owald, D., Perisse, E., Krashes, M.J., Das, G., Gohl, D.,
513 Silies, M., Certel, S., and Waddell, S. (2012). Layered reward signalling through
514 octopamine and dopamine in Drosophila. Nature *492*, 433-437.

515 6. Tully, T., Preat, T., Boynton, S.C., and Del Vecchio, M. (1994). Genetic dissection of
516 consolidated memory in Drosophila. Cell *79*, 35-47.

517 7. Bailey, C.H., Bartsch, D., and Kandel, E.R. (1996). Toward a molecular definition of
518 long-term memory storage. Proc Natl Acad Sci U S A *93*, 13445-13452.

519 8. Dubnau, J., and Chiang, A.S. (2013). Systems memory consolidation in Drosophila.
520 Curr Opin Neurobiol *23*, 84-91.

521 9. Cervantes-Sandoval, I., Martin-Pena, A., Berry, J.A., and Davis, R.L. (2013). System-like
522 consolidation of olfactory memories in Drosophila. J Neurosci *33*, 9846-9854.

523 10. Kitamura, T., and Ogawa, S.K. (2017). Engrams and circuits crucial for systems
524 consolidation of a memory. *356*, 73-78.

525 11. Caroni, P., Donato, F., and Muller, D. (2012). Structural plasticity upon learning:
526 regulation and functions. Nat Rev Neurosci *13*, 478-490.

527 12. Holtmaat, A., and Caroni, P. (2016). Functional and structural underpinnings of
528 neuronal assembly formation in learning. Nat Neurosci *19*, 1553-1562.

529 13. Kleim, J.A., Freeman, J.H., Jr., Bruneau, R., Nolan, B.C., Cooper, N.R., Zook, A., and
530 Walters, D. (2002). Synapse formation is associated with memory storage in the
531 cerebellum. Proc Natl Acad Sci U S A *99*, 13228-13231.

532 14. Hihara, S., Notoya, T., Tanaka, M., Ichinose, S., Ojima, H., Obayashi, S., Fujii, N., and
533 Iriki, A. (2006). Extension of corticocortical afferents into the anterior bank of the
534 intraparietal sulcus by tool-use training in adult monkeys. Neuropsychologia *44*,
535 2636-2646.

536 15. Bassett, D.S., Wymbs, N.F., Porter, M.A., Mucha, P.J., Carlson, J.M., and Grafton, S.T.
537 (2011). Dynamic reconfiguration of human brain networks during learning. Proc Natl
538 Acad Sci U S A *108*, 7641-7646.

539 16. Gu, S., Pasqualetti, F., Cieslak, M., Telesford, Q.K., Yu, A.B., Kahn, A.E., Medaglia, J.D.,
540 Vettel, J.M., Miller, M.B., Grafton, S.T., et al. (2015). Controllability of structural brain
541 networks. Nat Commun *6*, 8414.

542 17. Maviel, T., Durkin, T.P., Menzaghi, F., and Bontempi, B. (2004). Sites of neocortical
543 reorganization critical for remote spatial memory. Science (New York, N.Y.) *305*, 96-
544 99.

545 18. Chklovskii, D.B., Mel, B.W., and Svoboda, K. (2004). Cortical rewiring and information
546 storage. Nature *431*, 782-788.

547 19. Gogolla, N., Galimberti, I., and Caroni, P. (2007). Structural plasticity of axon
548 terminals in the adult. Curr Opin Neurobiol *17*, 516-524.

549 20. Bennett, S.H., Kirby, A.J., and Finnerty, G.T. (2018). Rewiring the connectome:
550 Evidence and effects. Neurosci Biobehav Rev *88*, 51-62.

551 21. Boele, H.J., Koekkoek, S.K., De Zeeuw, C.I., and Ruigrok, T.J. (2013). Axonal sprouting
552 and formation of terminals in the adult cerebellum during associative motor learning.
553 J Neurosci *33*, 17897-17907.

554 22. Chen, J.L., Margolis, D.J., Stankov, A., Sumanovski, L.T., Schneider, B.L., and
555 Helmchen, F. (2015). Pathway-specific reorganization of projection neurons in
556 somatosensory cortex during learning. Nat Neurosci *18*, 1101-1108.

557 23. Poort, J., Khan, A.G., Pachitariu, M., Nemri, A., Orsolic, I., Krupic, J., Bauza, M., Sahani,
558 M., Keller, G.B., Mrsic-Flogel, T.D., et al. (2015). Learning Enhances Sensory and
559 Multiple Non-sensory Representations in Primary Visual Cortex. Neuron *86*, 1478-
560 1490.

561 24. Grewe, B.F., Grundemann, J., Kitch, L.J., Lecoq, J.A., Parker, J.G., Marshall, J.D., Larkin,
562 M.C., Jercog, P.E., Grenier, F., Li, J.Z., et al. (2017). Neural ensemble dynamics
563 underlying a long-term associative memory. Nature *543*, 670-675.

564 25. de Belle, J.S., and Heisenberg, M. (1994). Associative odor learning in Drosophila
565 abolished by chemical ablation of mushroom bodies. Science *263*, 692-695.

566 26. Butcher, N.J., Friedrich, A.B., Lu, Z., Tanimoto, H., and Meinertzhagen, I.A. (2012).
567 Different classes of input and output neurons reveal new features in microglomeruli
568 of the adult Drosophila mushroom body calyx. J Comp Neurol *520*, 2185-2201.

569 27. Caron, S.J., Ruta, V., Abbott, L.F., and Axel, R. (2013). Random convergence of
570 olfactory inputs in the Drosophila mushroom body. Nature *497*, 113-117.

571 28. Yasuyama, K., Meinertzhagen, I.A., and Schurmann, F.W. (2002). Synaptic
572 organization of the mushroom body calyx in Drosophila melanogaster. J Comp Neurol
573 *445*, 211-226.

574 29. Kremer, M.C., Christiansen, F., Leiss, F., Paehler, M., Knapek, S., Andlauer, T.F.,
575 Forstner, F., Kloppenburg, P., Sigrist, S.J., and Tavosanis, G. (2010). Structural long-
576 term changes at mushroom body input synapses. Curr Biol *20*, 1938-1944.

577 30. Pech, U., Revelo, N.H., Seitz, K.J., Rizzoli, S.O., and Fiala, A. (2015). Optical dissection
578 of experience-dependent pre- and postsynaptic plasticity in the Drosophila brain. Cell
579 Rep *10*, 2083-2095.

580 31. Leiss, F., Groh, C., Butcher, N.J., Meinertzhagen, I.A., and Tavosanis, G. (2009).
581 Synaptic organization in the adult Drosophila mushroom body calyx. J Comp Neurol
582 *517*, 808-824.

583 32. Datta, S.R., Vasconcelos, M.L., Ruta, V., Luo, S., Wong, A., Demir, E., Flores, J.,
584 Balonze, K., Dickson, B.J., and Axel, R. (2008). The Drosophila pheromone cVA
585 activates a sexually dimorphic neural circuit. Nature *452*, 473-477.

586 33. Kurtovic, A., Widmer, A., and Dickson, B.J. (2007). A single class of olfactory neurons
587 mediates behavioural responses to a Drosophila sex pheromone. Nature *446*, 542-
588 546.

589 34. Schlief, M.L., and Wilson, R.I. (2007). Olfactory processing and behavior downstream
590 from highly selective receptor neurons. Nat Neurosci *10*, 623-630.

591 35. Lebreton, S., Grabe, V., Omondi, A.B., Ignell, R., Becher, P.G., Hansson, B.S., Sachse,
592 S., and Witzgall, P. (2014). Love makes smell blind: mating suppresses pheromone
593 attraction in Drosophila females via Or65a olfactory neurons. Sci Rep *4*, 7119.

594 36. Lebreton, S., Trona, F., Borrero-Echeverry, F., Bilz, F., Grabe, V., Becher, P.G.,
595 Carlsson, M.A., Nässel, D.R., Hansson, B.S., Sachse, S., et al. (2015). Feeding regulates
596 sex pheromone attraction and courtship in Drosophila females. Scientific Reports *5*,
597 13132.

598 37. Zheng, Z., Lauritzen, J.S., Perlman, E., Robinson, C.G., Nichols, M., Milkie, D., Torrens,
599 O., Price, J., Fisher, C.B., Sharifi, N., et al. (2018). A Complete Electron Microscopy
600 Volume of the Brain of Adult Drosophila melanogaster. Cell *174*, 730-743 e722.

601 38. Aso, Y., Hattori, D., Yu, Y., Johnston, R.M., Iyer, N.A., Ngo, T.T., Dionne, H., Abbott,
602 L.F., Axel, R., Tanimoto, H., et al. (2014). The neuronal architecture of the mushroom
603 body provides a logic for associative learning. Elife *3*, e04577.

604 39. Lin, H.H., Lai, J.S., Chin, A.L., Chen, Y.C., and Chiang, A.S. (2007). A map of olfactory
605 representation in the Drosophila mushroom body. Cell *128*, 1205-1217.

606 40. Liu, X., and Davis, R.L. (2009). The GABAergic anterior paired lateral neuron
607 suppresses and is suppressed by olfactory learning. Nat Neurosci *12*, 53-59.

608 41. Schmid, A., Hallermann, S., Kittel, R.J., Khorramshahi, O., Frolich, A.M., Quentin, C.,
609 Rasse, T.M., Mertel, S., Heckmann, M., and Sigrist, S.J. (2008). Activity-dependent
610 site-specific changes of glutamate receptor composition in vivo. Nat Neurosci *11*,
611 659-666.

612 42. Tempel, B.L., Bonini, N., Dawson, D.R., and Quinn, W.G. (1983). Reward learning in
613 normal and mutant Drosophila. Proc Natl Acad Sci U S A *80*, 1482-1486.

614 43. Bhandawat, V., Olsen, S.R., Gouwens, N.W., Schlief, M.L., and Wilson, R.I. (2007).
615 Sensory processing in the Drosophila antennal lobe increases reliability and
616 separability of ensemble odor representations. Nat Neurosci *10*, 1474-1482.

617 44. Pohl, J.B., Baldwin, B.A., Dinh, B.L., Rahman, P., Smerek, D., Prado, F.J., Sherazee, N.,
618 and Atkinson, N.S. (2012). Ethanol preference in Drosophila melanogaster is driven
619 by its caloric value. Alcoholism, clinical and experimental research *36*, 1903-1912.

620 45. Levin, L.R., Han, P.L., Hwang, P.M., Feinstein, P.G., Davis, R.L., and Reed, R.R. (1992).
621 The Drosophila learning and memory gene rutabaga encodes a Ca2+/Calmodulin-
622 responsive adenylyl cyclase. Cell *68*, 479-489.

623 46. Thum, A.S., Jenett, A., Ito, K., Heisenberg, M., and Tanimoto, H. (2007). Multiple
624 memory traces for olfactory reward learning in Drosophila. J Neurosci *27*, 11132-
625 11138.

626 47. Lagasse, F., Devaud, J.M., and Mery, F. (2009). A switch from cycloheximide-resistant
627 consolidated memory to cycloheximide-sensitive reconsolidation and extinction in
628 Drosophila. J Neurosci *29*, 2225-2230.

629 48. Davis, R.L. (2011). Traces of Drosophila memory. Neuron *70*, 8-19.

630 49. Han, P.L., Levin, L.R., Reed, R.R., and Davis, R.L. (1992). Preferential expression of the
631 Drosophila rutabaga gene in mushroom bodies, neural centers for learning in insects.
632 Neuron *9*, 619-627.

633 50. Jenett, A., Rubin, G.M., Ngo, T.T., Shepherd, D., Murphy, C., Dionne, H., Pfeiffer, B.D.,
634 Cavallaro, A., Hall, D., Jeter, J., et al. (2012). A GAL4-driver line resource for
635 Drosophila neurobiology. Cell Rep *2*, 991-1001.

636 51. Clark, P.J., and Evans, F.C. (1954). Distance to nearest neighbour as a measure of
637 spatial relationships in populations. Ecology *35*, 445-453.

638 52. Jefferis, G.S., Potter, C.J., Chan, A.M., Marin, E.C., Rohlfing, T., Maurer, C.R., Jr., and
639 Luo, L. (2007). Comprehensive maps of Drosophila higher olfactory centers: spatially
640 segregated fruit and pheromone representation. Cell *128*, 1187-1203.

641 53. Ichinose, T., Aso, Y., Yamagata, N., Abe, A., Rubin, G.M., and Tanimoto, H. (2015).
642 Reward signal in a recurrent circuit drives appetitive long-term memory formation.
643 Elife *4*, e10719.

644 54. Cognigni, P., Felsenberg, J., and Waddell, S. (2018). Do the right thing: neural network
645 mechanisms of memory formation, expression and update in Drosophila. Curr Opin
646 Neurobiol *49*, 51-58.

647 55. Mao, Z., and Davis, R.L. (2009). Eight different types of dopaminergic neurons
648 innervate the Drosophila mushroom body neuropil: anatomical and physiological
649 heterogeneity. Front Neural Circuits *3*, 5.

650 56. Chen, C.C., Wu, J.K., Lin, H.W., Pai, T.P., Fu, T.F., Wu, C.L., Tully, T., and Chiang, A.S.
651 (2012). Visualizing long-term memory formation in two neurons of the Drosophila
652 brain. Science *335*, 678-685.

653 57. Busch, S., Selcho, M., Ito, K., and Tanimoto, H. (2009). A map of octopaminergic
654 neurons in the Drosophila brain. J Comp Neurol *513*, 643-667.

655 58. Boto, T., Stahl, A., Zhang, X., Louis, T., and Tomchik, S.M. (2019). Independent
656 Contributions of Discrete Dopaminergic Circuits to Cellular Plasticity, Memory
657 Strength, and Valence in Drosophila. Cell Rep *27*, 2014-2021 e2012.

658 59. Warth Perez Arias, C.C., Frosch, P., Fiala, A., and Riemensperger, T.D. (2020).
659 Stochastic and Arbitrarily Generated Input Patterns to the Mushroom Bodies Can
660 Serve as Conditioned Stimuli in Drosophila. Front Physiol *11*, 53.

661 60. Hourcade, B., Muenz, T.S., Sandoz, J.C., Rossler, W., and Devaud, J.M. (2010). Long-
662 term memory leads to synaptic reorganization in the mushroom bodies: a memory
663 trace in the insect brain? J Neurosci *30*, 6461-6465.

664 61. Falibene, A., Roces, F., and Rossler, W. (2015). Long-term avoidance memory
665 formation is associated with a transient increase in mushroom body synaptic
666 complexes in leaf-cutting ants. Front Behav Neurosci *9*, 84.

667 62. Gupta, N., and Stopfer, M. (2014). A temporal channel for information in sparse
668 sensory coding. Curr Biol *24*, 2247-2256.

669 63. Haenicke, J., Yamagata, N., Zwaka, H., Nawrot, M., and Menzel, R. (2018). Neural
670 Correlates of Odor Learning in the Presynaptic Microglomerular Circuitry in the
671 Honeybee Mushroom Body Calyx. eNeuro *5*.

672 64. Gruntman, E., and Turner, G.C. (2013). Integration of the olfactory code across
673 dendritic claws of single mushroom body neurons. Nat Neurosci *16*, 1821-1829.

674 65. Delestro, F., Scheunemann, L., Pedrazzani, M., Tchenio, P., Preat, T., and Genovesio,
675 A. (2020). In vivo large-scale analysis of Drosophila neuronal calcium traces by
676 automated tracking of single somata. Scientific Reports *10*, 7153.

677 66. Saalfeld, S., Cardona, A., Hartenstein, V., and Tomancak, P. (2009). CATMAID:
678 collaborative annotation toolkit for massive amounts of image data. Bioinformatics
679 *25*, 1984-1986.

680 67. Prokop, A., and Meinertzhagen, I.A. (2006). Development and structure of synaptic
681 contacts in Drosophila. Semin Cell Dev Biol *17*, 20-30.

682 68. Tanaka, N.K., Tanimoto, H., and Ito, K. (2008). Neuronal assemblies of the Drosophila
683 mushroom body. J Comp Neurol *508*, 711-755.

684 69. Grabe, V., Strutz, A., Baschwitz, A., Hansson, B.S., and Sachse, S. (2015). Digital in vivo
685 3D atlas of the antennal lobe of Drosophila melanogaster. J Comp Neurol *523*, 530-
686 544.

687 70. Costa, M., Manton, J.D., Ostrovsky, A.D., Prohaska, S., and Jefferis, G.S. (2016).
688 NBLAST: Rapid, Sensitive Comparison of Neuronal Structure and Construction of
689 Neuron Family Databases. Neuron *91*, 293-311.

690 71. Cardona, A., Saalfeld, S., Schindelin, J., Arganda-Carreras, I., Preibisch, S., Longair, M.,
691 Tomancak, P., Hartenstein, V., and Douglas, R.J. (2012). TrakEM2 software for neural
692 circuit reconstruction. PLoS One *7*, e38011.

693 72. Cuntz, H., Forstner, F., Borst, A., and Hausser, M. (2011). The TREES toolbox--probing
694 the basis of axonal and dendritic branching. Neuroinformatics *9*, 91-96.

695 73. Schindelin, J., Arganda-Carreras, I., Frise, E., Kaynig, V., Longair, M., Pietzsch, T.,
696 Preibisch, S., Rueden, C., Saalfeld, S., Schmid, B., et al. (2012). Fiji: an open-source
697 platform for biological-image analysis. Nat Methods *9*, 676-682.

698 74. Louis, T., Stahl, A., Boto, T., and Tomchik, S.M. (2018). Cyclic AMP-dependent
699 plasticity underlies rapid changes in odor coding associated with reward learning.
700 Proc Natl Acad Sci U S A *115*, E448-E457.

701 75. Thevenaz, P., Ruttimann, U.E., and Unser, M. (1998). A pyramid approach to subpixel
702 registration based on intensity. IEEE Trans Image Process *7*, 27-41.

703